

Additive Manufacturing

Characterization of additive-manufactured TPMS structures under compressive loading by means of energy-absorption diagram

--Manuscript Draft--

Manuscript Number:	
Article Type:	Research Paper
Keywords:	Lattice; additive manufacturing; compression; triply periodic minimal surface structures; energy absorption
Corresponding Author:	Ramon Miralbes, Ph.D. Universidad de Zaragoza Escuela de Ingeniería y Arquitectura Zaragoza, Aragón SPAIN
First Author:	Ramon Miralbes, Ph.D.
Order of Authors:	Ramon Miralbes, Ph.D. David Ranz, Dr. Francisco Javier Pascual, Dr. Dimitrios Zouzias Jose Antonio Gomez
Abstract:	Triply periodic minimal surface structures (TPMS) can create tailored complex structures that could be a substitute for polymeric foams in certain applications, owing to the advantages of additive manufacturing processes. The main application is the absorption of energy under compression loads. Consequently, it is necessary to study the different types of TPMS structures (Neovious, gyroid, Schwarz-P, Lidinoid, split-P, and diamond) to analyze them in terms of their energy-absorbing capability, mechanical properties, effectivity, ideality, etc. Additionally, it is necessary to compare them in terms of volume and in terms of weight using the specific properties.
Suggested Reviewers:	Siamak F. Khosroshahi s.f.khosroshahi@imperial.ac.uk Expert in TPMS mechanical characterization Ajit Panesar a.panesar@imperial.ac.uk Expert in Lattice structures and CAD model of them Nathan B. Crane ncrane@usf.edu Expert in diamond TPMS structures

1
2
3
4
5
6
7
8
9
10
11
12
13
14
15
16
17
18
19
20
21
22
23
24
25
26
27
28
29
30
31
32
33
34
35
36
37
38
39
40
41
42
43
44
45
46
47
48
49
50
51
52
53
54
55
56
57
58
59
60
61
62
63
64
65

- Triply periodic minimal surface structures
- Material properties under compression loads
- Energy Absorption capability of TPMS
- Characterization using energy diagrams
- Substitution of EPS to TPMS in helmets
- Compression comparative behavior

CHARACTERIZATION OF ADDITIVE-MANUFACTURED TPMS STRUCTURES UNDER COMPRESSIVE LOADING BY MEANS OF ENERGY-ABSORPTION DIAGRAM

Abstract

Triply periodic minimal surface structures (TPMS) can create tailored complex structures that could be a substitute for polymeric foams in certain applications, owing to the advantages of additive manufacturing processes. The main application is the absorption of energy under compression loads. Consequently, it is necessary to study the different types of TPMS structures (Neovious, gyroid, Schwarz-P, Lidinoid, split-P, and diamond) to analyze them in terms of their energy-absorbing capability, mechanical properties, effectivity, ideality, etc. Additionally, it is necessary to compare them in terms of volume and in terms of weight using the specific properties.

Moreover, there are many different diagrams that can be used to compare materials, such as the stress–strain or the effectivity–stress diagrams, and many different indices, such as the ideality, effectivity, and total effectivity. Therefore, it is necessary to use them to analyze the main conclusions and uses that can be achieved with each TPMS structure.

1. Introduction

The automotive and packaging industries have widely used polymeric foams such as expanded polystyrene (EPS) to absorb energy and prevent injuries to the occupants of a vehicle in case of impact or to prevent damage to goods. These materials have excellent energy dissipation properties and, additionally, they are economic, have low density, and can be used to generate any geometric complex parts. Therefore, they have been used in diverse applications such as liners in helmets (for work, sports, etc.), seat cushions, side impact protection systems, and bumper systems.

Polymeric foams are created during a foaming process, in which it is possible to control the expansion of the foam to obtain the desired density. The relationship between the density and the mechanical properties is well-known, especially under compression efforts [1,2]. Here, it must be noted that foams under compression efforts have characteristic stress–strain curves. These curves could be defined using the Gibson model [3] in three well-defined parts, depending on the density of the material. The first of these zones is a linear zone that has a linear elastic behavior with the slope of the elastic Young's modulus of the material. Afterwards, in the plateau zone, the cells begin to collapse, which progresses at roughly constant load. In this zone, the stress levels increase slowly, which defines the plateau Young's modulus. Finally, the densification zone appears when the opposing walls of the cells meet and touch, the densification occurs, and consequently the stress increases steeply. (See fig. 1).

Owing to the shapes of the stress–strain curves, the main parameters are:

- Maximum tensile strength in the elastic zone ($\sigma_{c,e}$)
- Maximum tensile strength in the densification point ($\sigma_{c,d}$)
- Maximum elastic elongation ($\epsilon_{c,p}$)
- Elongation in the densification point ($\epsilon_{c,d}$)
- Elastic Young's modulus (E_c)
- Plateau Young's modulus (E_p)

The energy can be obtained from the following equation:

$$W = \int_0^{\varepsilon} \sigma(\varepsilon) d\varepsilon \quad (1)$$

Consequently, they appear the different absorbed energies:

- Elastic absorber energy $W_e = \int_0^{\varepsilon_{c,p}} \sigma(\varepsilon) d\varepsilon \quad (2)$

- Energy absorber in the plateau zone $W_p = \int_{\varepsilon_{c,p}}^{\varepsilon_{c,d}} \sigma(\varepsilon) d\varepsilon \quad (3)$

Using the density (ρ), it possible to obtain the specific properties, which are given by the ratio of the previous parameters to the density. Whereas nonspecific parameters are used to compare different materials with the same volume, specific parameters are used to compare materials with the same weight. Then, the following parameters are obtained:

- Maximum specific tensile strength in the elastic zone ($\sigma_{cs,e}$)
- Maximum specific tensile strength in the densification point ($\sigma_{cs,d}$)
- Specific elastic Young's modulus (E_{cs})
- Specific plateau Young's modulus (E_{ps})
- Specific elastic absorbed energy (W_{es})
- Specific energy absorbed in the plateau zone (W_{ps})

There are certain considerations that are involved in the design of an effective energy absorber, such as the geometry of the protection device, which has a notable influence on the load transfer but the most meaningful consideration is the material to be employed. Despite the fact that traditional polymeric foams are suitable for such applications, the limits of this material to absorb energy have been reached, especially in single-density EPS designs. One of the reasons for this is that, in the case of helmets, each part of the head has a different tolerance to damage and deceleration [4] and there are different impact probabilities in different zones of the helmet [5]; consequently, there are zones of the helmet that must have higher absorption capability and others that should have lower ones. In the same way, it has recently been discovered that the rotational moments and decelerations of the head under oblique impacts [6] have a high influence on the brain damage, and the reduction in weight of the helmet is essential to reduce these moments.

Consequently, different strategies are being studied to overcome the mentioned drawbacks, such as the use of different densities in the same helmets [7], the use of other materials such as cork and cork agglomerates [8,9], and the use of composite materials in liners [10].

One of these initiatives is based on the options that new additive manufacturing (AM) processes offer [11]. These technologies enable tailoring mechanical properties, such that it is possible to generate zones with differentiated stiffness that can be optimized to improve safety and reduce weight. This is based on the principle of using different infill materials and optimizing them to improve the safety of helmets. In this way, different types of fillings have been studied, such as prismatic tetrahedral [11], trust [12], bio-inspired structures [13], and auxetic lattices [14].

One of the possible types of structures that can be printed are the triply periodic minimal surface (TPMS) structures, which are invariant under a rank-3 translation and are commonly known as lattice structures. These structures, which imitate nature [15], are intricate periodic forms that are characterized by their effectivity to absorbed energy under compression loads and their inherit lightweight nature [16]. Hence, these structures could be optimal to substitute polymeric foams owing to their characteristics and the possibility that AM offers to

1 tailor them and adapt their stiffness across a helmet to optimize weight and protection.
2 Additionally, the development of AM allows the application of a wide variety of materials and
3 the use of TPMS has been noted in some of them, including stainless steel [17], thermoplastics
4 [18], titanium [19], natural-origin materials, and elastomers [20], so the possibilities to
5 customize the materials are nearly unlimited.

6
7 There are many different types of TPMS structures, but some of the most promising ones in
8 terms of specific mechanical properties are the gyroid, diamond, Schwarz-P or primitive,
9 Lidinoid, Neovious, and split-P [21, 22, 23].

10
11 Some studies have comparatively analyzed a few of these structures, such as the work of
12 Podrouzek. J. [24] that compares Schwarz-P, Schwarz-D, and gyroid under compression efforts
13 generated using a conventional layer-based fused deposition modeling (FDM). The main
14 conclusions are the similar specific mechanical behavior between the gyroid and Schwarz-P
15 and the lower properties of the Schwarz-D. Yu, S. [25] studied uniform and graded PLA gyroid
16 and Schwarz-P structures generated using FDM techniques. The main conclusion was that,
17 although the stress–strain curves were completely different, there were not many differences
18 in terms of the energy absorbed and they were similar to honeycomb structures.

19
20 It must be pointed out here that the main parameters that geometrically define a TPMS
21 structure are usually the unit cell length and the thickness of the walls or the structural
22 porosity. The structures are generated using mathematical equations that generate the surface
23 and, subsequently, they are thickened to obtain the final geometry.

24
25 An additional method to tailor the mechanical properties of these materials, especially the
26 stress–strain curve, is based on the generation of nonuniform-porosity structures called
27 functionally graded lattice structures [26, 23]. Then, it is possible, for instance, to create a
28 constantly increasing curve [25].

29
30 This article will be focused on the study of the main promising TPMS structures under
31 compression loads, generated using FDM techniques and different materials. This will give a
32 broad view of the mechanical behavior of these materials that could be used to select the
33 desirable material and structure to generate improved and customized materials to substitute
34 polymeric foams.

35 **2. Materials and Methods**

36 **2.1. Materials**

37 The material to be studied is an acrylonitrile butadiene styrene with the commercial name Z-
38 ULTRAT. All the specimens were printed using a fused filament fabrication (FFF) procedure
39 with a Zortrax M200 printer, using a 0.4-mm nozzle with a layer height of 0.19 mm.

40 The solid materials were tested under compression efforts according with the ASTM D1621
41 test method to obtain the main mechanical properties and material curves that will be used to
42 compare with the lattice structures. (see fig. 3).

43 Additionally, a reference EPS with a density of 120 kg/m^3 was tested according ASTM D1621
44 (see fig. 3).

45 In this study, six different TPMS structures generated using the nTopology software package
46 are tested, which are the gyroid, Schwarz P, Lidinoid, Neovious, diamond, and split-P (see fig.
47
48
49
50
51
52
53
54
55
56
57
58
59
60
61
62
63
64
65

2). Please note that previous studies have shown that these structures have a similar stress–strain curve to the polymeric foams [22, 23, 24, 25, 26].

2.2. Methods

The materials were studied under quasistatic compression using an 8032 INSTRON universal test machine with a 5 mm/min velocity for the compression test. There is not a specific standard to test such lattice structures, but their mechanical behavior is similar for the tested materials to a cellular foam, such as EPS or poly urethane (PUR). Consequently, with this type of material, they can be tested according to, for instance, the standard ASTM D1621 “Standard Test Method for Compressive Properties of Rigid Cellular Plastics,” the ISO 844 “Rigid Cellular Plastics Compression Properties,” or the ASTM 3574 “Standard Test Methods for Flexible Cellular Materials-Slab, Bonded, and Molded Urethane Foams.”

In the case of ASTM D1621, the minimum specimen has dimensions of $25.4 \times 25.4 \times 25.4 \text{ mm}^3$, for ISO 844, the minimum thickness is 50 mm and the preferred specimen is a $50 \times 100 \times 100 \text{ mm}^3$ prism, and finally in ASTM 3574, the preferred dimensions are a prism of $50 \times 50 \times 25 \text{ mm}^3$. Finally, it was decided to use the ASTM D1621 test with a $50 \times 50 \times 50 \text{ mm}^3$ prism specimen for the lattice structures and a $25.4 \times 25.4 \times 25.4 \text{ mm}^3$ prism for the solid specimens and for the EPS120 used to characterize the solid material. It was decided to use this standard and these sizes based on the maximum load capability of the test machine.

It must be mentioned here that the size of the specimens was used to determine the period of the lattice structures, which was set to 5 mm. Hence, there are 10 cells in each direction, which will avoid any distortion due to a low number of cells. Additionally, the specimen thickness was set to normalize the specimens with the same thickness in the program. However, this supposed that the specimens had different relative densities. It must be highlighted here that the nTopology software has certain limitations of the thickness. This supposes for instance that, for certain TPMS structures, it is impossible to reduce the thickness (such as for the split-P and the Neovious structures) and in other cases it is not possible to increase the thickness to certain a point. Hence, it is impossible to obtain weight-normalized specimens and the specimens were therefore normalized a thickness of 1. The final relative densities of the materials are listed in table 1.

The forces and displacements used to determine the stress–strain curve and the absorbed energy–strain curve were obtained from the INSTRON machine. By making use of these results as well as the density, the specific stress–strain curve and the specific absorbed energy–strain curve were obtained.

2.3. Interpretation of the results from testing of lattice structures

The aim of these types of structures is the absorption of energy to dissipate the kinetic energy of a shock and to maintain the maximum deceleration and/or force below a certain limit. The limit depends on the application, and thus in the case of the foams, it was possible to tailor the density and the thickness to obtain an approximated optimal behavior [3]. It is necessary here to explain the influence of the stress–strain curve on the maximum force, which is related to the deceleration. If the material does not have sufficient stiffness across the curve, especially in the plateau zone (low $\sigma_{c,e}$ and low W_p), then the densification zone is reached (strain higher than $\epsilon_{c,d}$) and, consequently, the stiffness increases exponentially. Finally, this implies that high forces and decelerations may occur that can exceed the limits and cause breakage of the goods in the case of packaging or severe brain injuries in the case of a helmet. However, if the

material is excessively stiff (high $\sigma_{c,e}$), then the initial stiffness at the plateau zone could be excessive (high forces and decelerations at the beginning) and, additionally, the final strain will be low such that the material will be only partially used. The objective is to optimize the material to use all of the plateau zone. Figure 5 shows that materials with different properties can absorb the same energy but the maximum stress and strain are different. Plotting the energy–stress demonstrates this fact and enables one to obtain the optimal energy absorption envelope to select the best material for each application. The right-hand figure shows the energy absorption–stress diagram proposed by Gibson L.J. [27]. This can be used to obtain the optimal envelope, which is useful to select the suitable material structure that gives the minimum stress.

Another way to present the results was proposed by Miltz J. [28], which used an additional indicator named the efficiency parameter (E). This parameter is the ratio of the absorbed energy to the stress, and it is usually plotted against the strain (fig. 3).

$$W = \frac{\int_0^\varepsilon \sigma(\varepsilon) d\varepsilon}{\sigma} \quad (4)$$

The typical efficiency–stress diagram for a foam always has a maximum because, after a certain point, the increase in the energy is lower than the increase in the absorbed energy. This can be easily understood by examining fig. 1 and fig. 4. In fig. 1 diagram it is possible to obtain the envelope (which is equivalent to that in fig. 4) that shows the optimal structures that maximize the absorbed energy. It must be pointed that, despite the fact that the energy–stress diagram and the efficiency–stress diagram are equivalent, the latter offers some advantages: it is more intuitive to use to compare and select materials that will have the highest efficiency to absorb energy without exceeding a certain stress.

However, some authors showed that the use of efficiency is questionable [29, 30]. They demonstrated that efficiency is useful for materials characterized by a monotonically increasing stress with strain. In other cases, if there is a relative maximum in an early stage that is sufficiently high, it is more suitable the use of the total efficiency. The total efficiency (W_t) is the ratio of the energy W to the maximum experienced stress; it should be noted that the total efficiency and efficiency are identical for monotonically increasing materials.

$$W_t = \frac{\int_0^\varepsilon \sigma(\varepsilon) d\varepsilon}{\max_{0 \leq x \leq \varepsilon} \sigma} \quad (5)$$

Miltz J. [28] proposed another indicator called the ideality (I), which was defined according as follows:

$$I = \frac{\int_0^\varepsilon \sigma(\varepsilon) d\varepsilon}{\sigma \varepsilon} \quad (6)$$

Ideality is a ratio of the efficiency that takes into consideration both the strain and the stress to analyze how close to an ideal absorber (one with a constant stress along the strain) is the material. Nevertheless, Miltz J. [28] noticed that despite the fact that this variable gives the optimal material for a given limited stress, the material suffered very low deformation, and thus it does not use all of the energy-absorbing capability across the plateau zone. As a result, it was proposed to use this variable to determine the lower limit to use a material adequately (which corresponds with the zone with the greater slope in the absorbed energy–stress diagram; see fig. 4)

1 It is common in lattice structures to use the normalized form [25, 31] that presents a double
2 logarithm diagram of the absorbed energy divided by the elastic modulus of the original
3 material in the elastic compression zone vs the stress divided by the elastic modulus of the
4 original material. In this particular case, the elastic modulus of the original material is equal for
5 all the specimens and the obtained diagram would be identical to the previously mentioned
6 absorbed energy vs stress diagram. This type of diagram would be useful to compare
7 structures with different materials.
8

9 There are other interesting parameters to compare the energy absorption capability of a foam
10 based on the Rush model [32, 33, 34], such as the Jansen factor [3] and the cushion factor [3],
11 but difficulties involving the mechanical characterization of the Rush model require further
12 efforts and prevent its use.
13
14

15 **3. Results and discussion**

16 Fig. 4 and table 1 show the stress–strain curves of all the specimens. It can be observed that
17 the Lidinoid structure presents a quasiconstant plateau whose shape is similar to that of EPS. In
18 the case of the diamond, at the beginning of the plateau there is a local maximum, after which
19 the stiffness reduces slightly. In the cases of the split-P, gyroid, and Schwarz-P, there is a stress
20 peak at the beginning of the plateau, after which there are some oscillations that are related
21 to the collapse of the cells in lines as Yu [25] indicated. It can be observed that the first
22 oscillations are significantly higher for the gyroid. Consequently, the structures in this zone are
23 farther from an ideal material. In the case of the Neovious, it can be observed that, with half of
24 the relative density of the solid material (Z-ULTRAT), it presents a higher strength and the
25 strain in the plateau zone is higher. Additionally, this material has a constantly increasing
26 stiffness in the plateau zone. It must be highlighted that this structure has a relative density
27 approximately 1.5 times higher than those of the other structures and the mechanical
28 properties are consequently higher, but they are approximately 3 and 5 times higher. It can
29 also be observed that the densification zone in these structures begins with a strain of
30 approximately 50 or 60%. Additionally, in the structures with higher stiffness in the plateau,
31 the densification zone appears earlier. This is a common phenomenon noted in polymeric
32 foams such as EPS [2]. It can be also observed that, with the same normalized thickness and
33 cell size, the results vary significantly.
34
35
36
37
38
39
40

41 In the case of the specific stress–strain diagram (see fig. 7 and table 2) that has been used to
42 normalize the structures in terms of weight, it can be observed that some structures present
43 higher specific stiffness than the EPS120. This is the case for Neovious, diamond, and split-P. In
44 the case of the Schwarz-P and gyroid, they initially present a higher $\sigma_{cs,e}$ but then decrease
45 below the EPS curve. In addition, they present some waves, such that their stiffness in the
46 plateau zone varies, which is not efficient for absorbing energy. In the case of the Lidinoid,
47 whereas it presents a flatter plateau zone, the densification begins earlier and steeply. It can
48 be observed in this figure, the densification appears earlier than in EPS. Finally, the Neovious
49 exhibits the highest specific stiffness and the lowest $\varepsilon_{c,d}$.
50
51
52

53 In terms of absorbed energy (see fig. 8), it can be observed that the Neovious and the solid
54 material, under a given strain, have approximately the same capacity to absorb energy. In the
55 case of the other materials, it can be observed the capacity of each structure to absorb energy
56 is less than that of the solid material under a given strain.
57
58

59 Analyzing the results in terms of normalized absorbed energy (see fig. 9) it can be observed
60 that the EPS120 and the solid material present the highest values owing to the definition of
61
62
63
64
65

1 this factor. In the relationship with the TPMS structures, it can be observed that, for small
2 normalized stress, which occurs in the elastic zone, all the materials have similar normalized
3 energy and can absorb approximately the same energy in the elastic zone. Afterwards, the
4 previously noted behavior can be observed: the Neovious presents the best capability to
5 absorb energy, followed by the split-P and the diamond that present similar behavior. The
6 Schwarz-P and the Lidinoid present a lower capability to absorb energy and, finally, the gyroid
7 presents the lowest energy-absorbing capability.
8

9 In terms of specific absorbed energy (see fig. 10), which is used to compare the capacity to
10 absorb energy of structures with the same weight, it can be observed that the Neovious has
11 the highest specific capacity to absorb energy; the diamond and the split-P have a similar
12 capacity to that of the solid material until the latter reaches its densification point. In the case
13 of the Lidinoid and the Schwarz-P, until they reach the densification point, they are similar to
14 the EPS120. Finally, the gyroid structure shows the lowest specific capacity.
15
16

17 Analyzing the effectivity (see fig. 11 and table 3) shows the stress (σ_E) and the strain (ϵ_E) in the
18 maximum point with maximum effectivity. It can be observed that the Schwarz-P presents the
19 highest effectivity. The Neovious, diamond, and gyroid present similar medium effectivity, but
20 with different stress and energy-absorption capability that is similar to that of the EPS. Finally,
21 the Lidinoid and the split-P present the lowest effectivity. In terms of the strain (see fig. 12), it
22 can be observed that the maximum effectivity is reached at the end of the plateau zone or at
23 the beginning of the densification zone. Consequently, this is an adequate index to compare
24 the different structures. In addition, it is possible to establish iso-energy curves in the diagram
25 to select the most effective energy absorber and similarly obtain the stress.
26
27
28
29

30 It was pointed that, if the stress is nonmonotonically increasing, then it is more suitable the
31 use of the total effectivity. See fig. 13, fig. 14, and table 3, which show the stress (σ_{Et}) and the
32 strain (ϵ_{Et}) in the maximum point with the maximum total effectivity.
33
34

35 In the case where the curves increase monotonically, the curves are identical to the effective
36 curves. Wide differences are apparent for the Schwarz-P and the gyroid and minimal
37 differences can be observed for the split-P. In terms of maximum values, in these cases, the
38 total efficiency is lower than the efficiency and σ_{Et} and ϵ_{Et} are higher: the Schwarz-P presents
39 the highest total efficiency but then it decrease to 45.2%; the stress at this point (σ_{Et}) increases
40 to 7.8 MPa and the ϵ_{Et} increase to 60.2%. In the case of the gyroid, the total efficiency
41 decreases from 41.7% to 36.5%; the stress at this point (σ_{Et}) increases to 7.7 MPa and the ϵ_{Et}
42 increases to 59.3%.
43
44

45 The study of the ideality (see fig. 15 and table 3) reveals that the gyroid presents by far the
46 highest ideality. The diamond presents a high ideality and the Neovious presents the lowest.
47 The highest ideality of the gyroid is related to the initial peak that appears in the stress–strain
48 curve, whereas the low ideality of the Neovious is related the shape of this curve in the elastic
49 zone.
50
51

52 It can be observed in fig. 16 that all the materials present the highest idealities with a strain of
53 approximately 0.1 and 0.3. Consequently, this index cannot be used to select a material,
54 because only a small part of the plateau zone is used. For high strains, the ideality of the gyroid
55 decreases dramatically. However, the other materials have smoother ideality–strain curves,
56 especially the diamond, EPS120, and Neovious. This is related to the fact that these materials
57 do not present peaks in the stress–strain curve.
58
59
60
61
62
63
64
65

4. Conclusions

This article provides highly valuable data about the mechanical behavior of different types of TPMS and the use of different diagrams and indices to analyze the results. Additionally, the results of an FFF solid brick of the same material and those of a high-density foam used in certain energy-absorbing applications such as helmets, have been presented.

The main conclusions drawn from this study are as follows:

- Despite the use of the same normalized variables to generate the TPMS, there are some differences in terms of weight that are associated with their respective geometry definitions. In this case, the Neovious and gyroid present the maximum and minimum relative densities, respectively.
- There are several differences in the stress–strain curves that, whilst they are lower for the specific stress–strain curves, are significant. It can be observed that the gyroid presents an initial high peak; similarly, the split-P and the Schwarz present peaks at the end of the elastic zone. These three structures present oscillations in the plateau zone that are caused by the collapse of cells. These collapses do not appear in the other structures (Lidinoïd, Neovious, and diamond). In the case of the diamond, there is a small initial peak and the stress decreases step-by-step in the first half of the plateau zone. In the case of the Neovious, it presents a constantly increasing stress in the plateau zone and the diamond presents a constant plateau.
- One drawback of TPMS structures, compared with EPS foams, is that they reach the densification point with a lower strain, such that the final design can crash less than an EPS structure.
- In the case of the use of these structures to create a protective device such as a helmet, high peaks and waves must be avoided, because they produce high forces and, consequently, high decelerations that can cause brain damage. Therefore, the Neovious, Lidinoïd, and diamond are more suitable.
- In terms of absorbed energy, it has been observed that the Neovious presents the highest normalized and specific capability. The diamond and the split-P also present remarkable properties and the gyroid presents the lowest ones. The Lidinoïd and the Schwarz-P present similar capability to that of the EPS.
- In terms of effectivity, the Schwarz-P presents the highest; and the Lidinoïd, diamond, and gyroid have a medium effectivity that is similar to that of the EPS. Finally, the Lidinoïd and split-P present the lowest effectivity.
- It must be highlighted here that the ideality is not a suitable index to select the optimal structure and the effectivity and total effectivity are more suitable. The latter, despite the complexity of its equation, is more adequate if there is a nonmonotonically increasing stress–strain curve.
- The effectivity–stress combined with the use of iso-energy curves is a useful tool to select a material depending on the energy per unit volume that is necessary to be absorbed, but it is also interesting to plot the other curves to analyze possible local peaks, waves, etc.

To summarize, the most suitable TPMS structures to use in a helmet are the Neovious and the diamond and, to a lesser extent, the Lidinoïd. It is necessary to tailor these structures for use in a helmet, including full-helmet drop test analysis according to the United States Department of

1 Transportation (DOT), SNELL, Fédération Internationale de Motocyclisme (FIM), or similar
2 standards, using numerical or/and experimental tools.

3 **Acknowledgements**

4
5 The author(s) disclose receipt of the following financial support for the research, authorship,
6 and/or publication of this article: This work was supported by the “University of Zaragoza-
7 Centro Universitario de la Defensa” joint Research Grant. (grant number UZCUD2019-TEC-04).
8

9 The authors would like to thank nTopology that provided the software that was essential to
10 prepare all the CAD models.
11

12 **References**

- 13
14 [1] Doroudiani S, Kortschot M.T., Polystyrene foams. III. Structure–tensile properties
15 relationships, Journal of applied polymer 90 (2003), <https://doi.org/10.1002/app.12806>
16
17 [2] Chen, W., Hao, H., Hughes, D., et al., Static and dynamic mechanical properties of expanded
18 polystyrene, Materials & Design 69 (2015), <https://doi.org/10.1016/j.matdes.2014.12.024>
19
20 [3] Gibson L.J., Ashby M.F., Cellular solids: structures and properties, 2nd ed. Cambridge UK:
21 Cambridge University Press (1997), <https://doi.org/10.1017/CBO9781139878326>
22
23 [4] Clark, J.M., Post, A., Hoshizaki, TB, et al., Distribution of Brain Strain in the Cerebrum for
24 Laboratory Impacts to Ice Hockey Goaltender Masks, Journal of Biomechanical Engineering-
25 Transactions of the ASME 140 (2018), 10.1115/1.4040605
26
27 [5] Connor, T. A., Clark, J.M., Jayamohan, J., et al., Do equestrian helmets prevent concussion?
28 A retrospective analysis of head injuries and helmet damage from real-world equestrian
29 accidents, Sports Medicine-Open 5 (2019), 10.1186/s40798-019-0193-0
30
31 [6] Pang, T.Y., Thai, K.T., McIntosh, A.S., et al., Head and neck responses in oblique motorcycle
32 helmet impacts: a novel laboratory test method, International Journal of Crashworthiness 16
33 (2019), 10.1080/13588265.2011.559799
34
35 [7] Mustafa, H., Pang, T. Y., Ellena, T., et al., Impact attenuation of user-centred bicycle helmet
36 design with different foam densities, Journal of Physics Conference Series 1150 (2019),
37 10.1088/1742-6596/1150/1/01204
38
39 [8] Wilhelm, J., Ptak, M., Rusiński, E, Simulated depiction of head and brain injuries in the
40 context of cellular based materials in passive safety devices. Scientific Journals of the Maritime
41 University of Szczecin (2017), 10.17402/222
42
43 [9] Fernandes, F.A.O., Alves de Sousa, R.J., Ptak, M., et al., Helmet Design Based on the
44 Optimization of Biocomposite Energy-Absorbing Liners under Multi-Impact Loading, Applied
45 Sciences-Basel 9 (2019), 10.3390/app9040735
46
47 [10] Coelho, R.M., Alves de Sousa, R.J., Fernandes, F.A.O., Teixeira-Dias, F., New composite
48 liners for energy absorption purposes, Materials and Design 43 (2012),
49 <https://doi.org/10.1016/j.matdes.2012.07.020>
50
51 [11] Khosroshahi, S.F., Duckworth, H., Galvanetto, U., et al., The effects of topology and
52 relative density of lattice liners on traumatic brain injury mitigation, Journal of Biomechanics
53 97 (2019), <https://doi.org/10.1007/BF02412150>.
54
55
56
57
58
59
60
61
62
63
64
65

- 1 [12] Khosroshahi, S.F., Tsampas, S.A., Galvanetto, U., Feasibility study on the use of a
2 hierarchical lattice architecture for helmet liners, *Materials Today Communications* 14 (2018),
3 10.1016/j.mtcomm.2018.02.002.
- 4 [13] Najmon, J.C., Jacob, D.J., Wood, Z.M., et al., Cellular Helmet Liner Design through Bio-
5 inspired Structures and Topology Optimization of Compliant Mechanism Lattices, *SAE*
6 *International Journal of Transportation Safety* 6 (2018), 10.4271/2018-01-1057
- 7 [14] Shepherd, T., Winwood, K., Venkatraman, P., et al., Validation of a Finite Element
8 Modeling Process for Auxetic Structures under Impact, *Physica Status Solidi B-Basic Solid State*
9 *Physics* (2020).
- 10 [15] du Plessis, A., Broeckhoven, C., Yadroitsava, I., et. Al., Beautiful and Functional: A Review
11 of Biomimetic Design in Additive Manufacturing, *Additive Manufacturing* 27 (2019),
12 <https://doi.org/10.1016/j.addma.2019.03.033>
- 13 [16] Zhang, L., Feih, S., Daynes, S., et. Al., Energy absorption characteristics of metallic triply
14 periodic minimal surface sheet structures under compressive loading, *Additive Manufacturing*
15 23 (2018), <https://doi.org/10.1016/j.addma.2018.08.007>
- 16 [17] Al-Ketan, O., Rowshan, R., Abu Al-Rub, R.K., Topology-mechanical property relationship of
17 3D printed strut, skeletal, and sheet based periodic metallic cellular materials, *Additive*
18 *Manufacturing*, 19 (2018), <https://doi.org/10.1016/j.addma.2017.12.006>.
- 19 [18] Bhandari, S., Lopez-Anido, R., Finite element analysis of thermoplastic polymer extrusion
20 3D printed material for mechanical property prediction, *Additive Manufacturing* 22 (2018),
21 <https://doi.org/10.1016/j.addma.2018.05.009>
- 22 [19] Choy, S.Y., Sun, C.N., Leong, K.F., Wei, J., Compressive properties of Ti-6Al-4V lattice
23 structures fabricated by selective laser melting: Design, orientation and density, *Additive*
24 *Manufacturing* 16 (2017), <https://doi.org/10.1016/j.addma.2017.06.012>
- 25 [20] Abayazid, F.F., Ghajari, M., Material characterisation of additively manufactured
26 elastomers at different strain rates and build orientations, *Additive Manufacturing* 33 (2018),
27 <https://doi.org/10.1016/j.addma.2020.101160>
- 28 [21] Maskerya, .I, Sturmb, L., Aremu, A.O., et. Al., Insights into the mechanical properties of
29 several triply periodic minimal surface lattice structures made by polymer additive
30 manufacturing, *Polymer* 152 (2018), <https://doi.org/10.1016/j.polymer.2017.11.049>
- 31 [22] Neff, C., Hopkinson, N., Crane, N.B., Experimental and analytical investigation of
32 mechanical behavior of laser-sintered diamond-lattice structures, *Additive Manufacturing* 22
33 (2018), <https://doi.org/10.1016/j.addma.2018.07.005>
- 34 [23] Panesar, A., Abdi, M., Hickman, D., et. Al., Strategies for functionally graded lattice
35 structures derived using topology optimisation for Additive Manufacturing, *Additive*
36 *Manufacturing* 19 (2018)
- 37 [24] Podrouzek, J., Marcon, M., Ninčević, K., et. Al, Bio-Inspired 3D Infill Patterns for Additive
38 Manufacturing and Structural Applications, *Materials (Basesl)* 12(2019), 10.3390/ma12030499
- 39 [25] Yu, S., Sun, J., Bai, J., Investigation of functionally graded TPMS structures fabricated by
40 additive manufacturing, *Materials & Design* 182 (2019),
41 <https://doi.org/10.1016/j.matdes.2019.108021>
- 42
43
44
45
46
47
48
49
50
51
52
53
54
55
56
57
58
59
60
61
62
63
64
65

- 1 [26] Nguyen, C.H.P., Kim, Y., Choi, Y., Design for Additive Manufacturing of Functionally Graded
2 Lattice Structures: A Design Method with Process Induced Anisotropy Consideration, Int. J. of
3 Precis. Eng. and Manuf.-Green Tech (2019), <https://doi.org/10.1007/s40684-019-00173-7>
- 4 [27] Avalle, M., Belingardi, G., Montanini, R., Characterization of polymeric structural foams
5 under compressive impact loading by means of energy-absorption diagram, International
6 Journal of Impact Engineering 25 (2001), [https://doi.org/10.1016/S0734-743X\(00\)00060-9](https://doi.org/10.1016/S0734-743X(00)00060-9)
- 7 [28] Miltz J., Ramon O., Energy absorption characteristics of polymeric foams used as
8 cushioning materials. Polymer Engineering Scien 30 (1990),
9 <https://doi.org/10.1002/pen.760300210>
- 10 [29] Hanssen A.G., Langseth M., Hopperstad O.S., Static and dynamic crushing of square
11 aluminium extrusions with aluminium foam, International Journal of Impact Engineering 24
12 (2000), [https://doi.org/10.1016/S0734-743X\(99\)00169-4](https://doi.org/10.1016/S0734-743X(99)00169-4)
- 13 [30] Hanssen A.G., Langseth M., Hopperstad O.S., Static crushing of square aluminium
14 extrusions with aluminium foam, International Journal of Mechanic Science 41 (1999),
15 [https://doi.org/10.1016/S0020-7403\(98\)00064-2](https://doi.org/10.1016/S0020-7403(98)00064-2)
- 16 [31] Maskery I., Aboulkhair N.T., Aremu A.O., et. Al., Compressive failure modes and energy
17 absorption in additivelymanufactured double gyroid lattices, Additive Manufacturing 16
18 (2017), <https://doi.org/10.1016/j.addma.2017.04.003>.
- 19 [32] Rush K.C., Load compression behavior of flexible foams, Journal of Applied Polymer
20 Science 13 (1969)
- 21 [33] Rush K.C., Energy-absorbing characteristics of foamed polymers. Journal of Applied
22 Polymer Science 14 (1970)
- 23 [34] Rush K.C., Load compression behavior of brittle foams, Journal of Applied Polymer Science
24 14 (1970)
- 25
26
27
28
29
30
31
32
33
34
35
36
37
38
39
40
41
42
43
44
45
46
47
48
49
50
51
52
53
54
55
56
57
58
59
60
61
62
63
64
65

Fig. 1. Typical stress-strain curve for the EPS

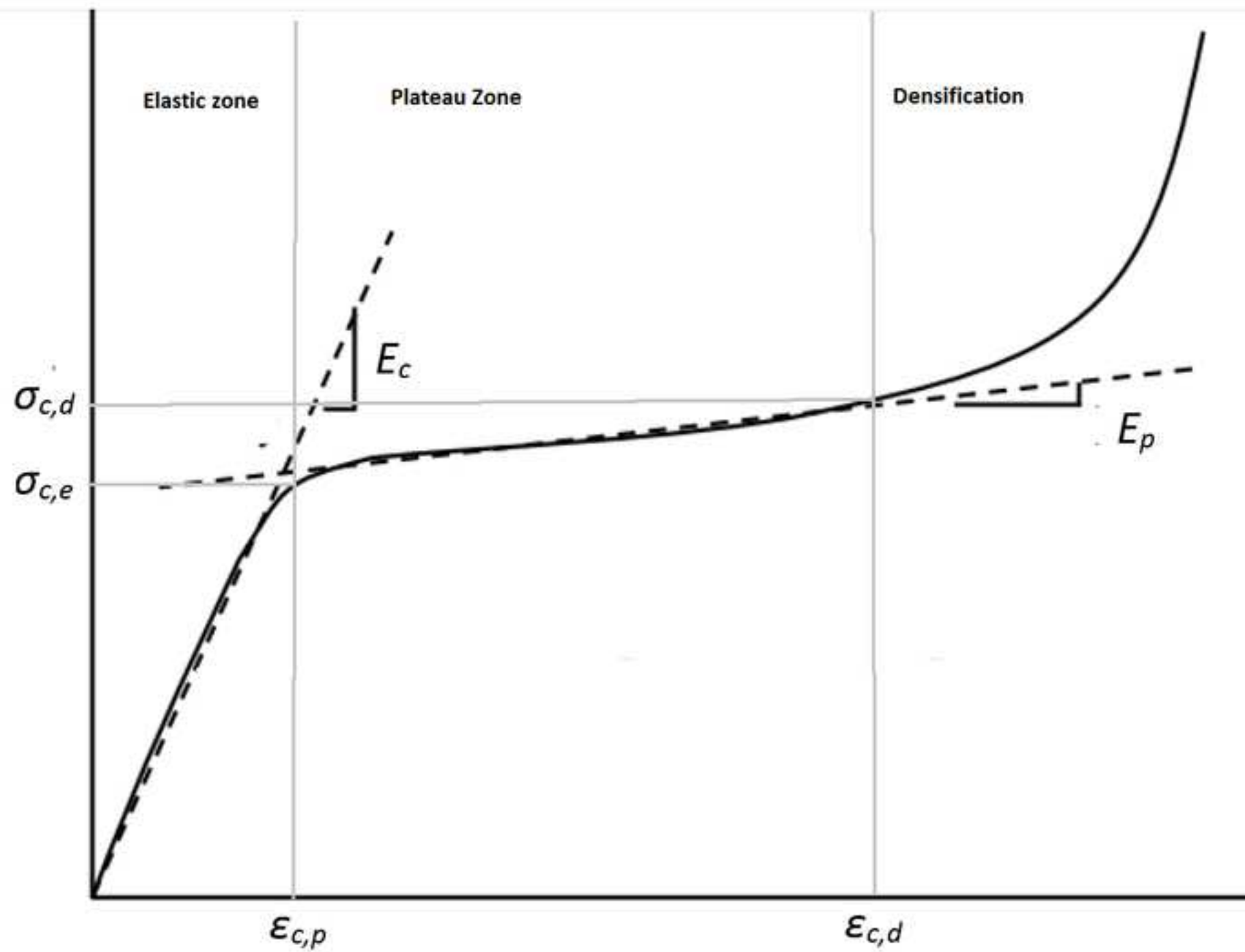


Fig. 2. From Left to the right: gyroid, Schwarz P, Lidinoid, Neovious, diamond, and split-P CAD models

[Click here to access/download;Figure;fig_2.bmp](#) 

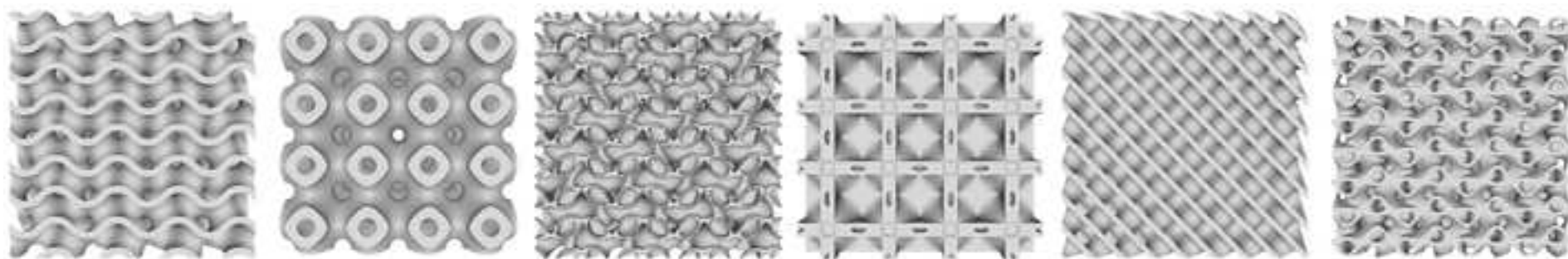


Fig. 3. Stress-strain compression curve for EPS120 and the Z-ULTRAT (ABS)

[Click here to access/download;Figure;fig_3.bmp](#)

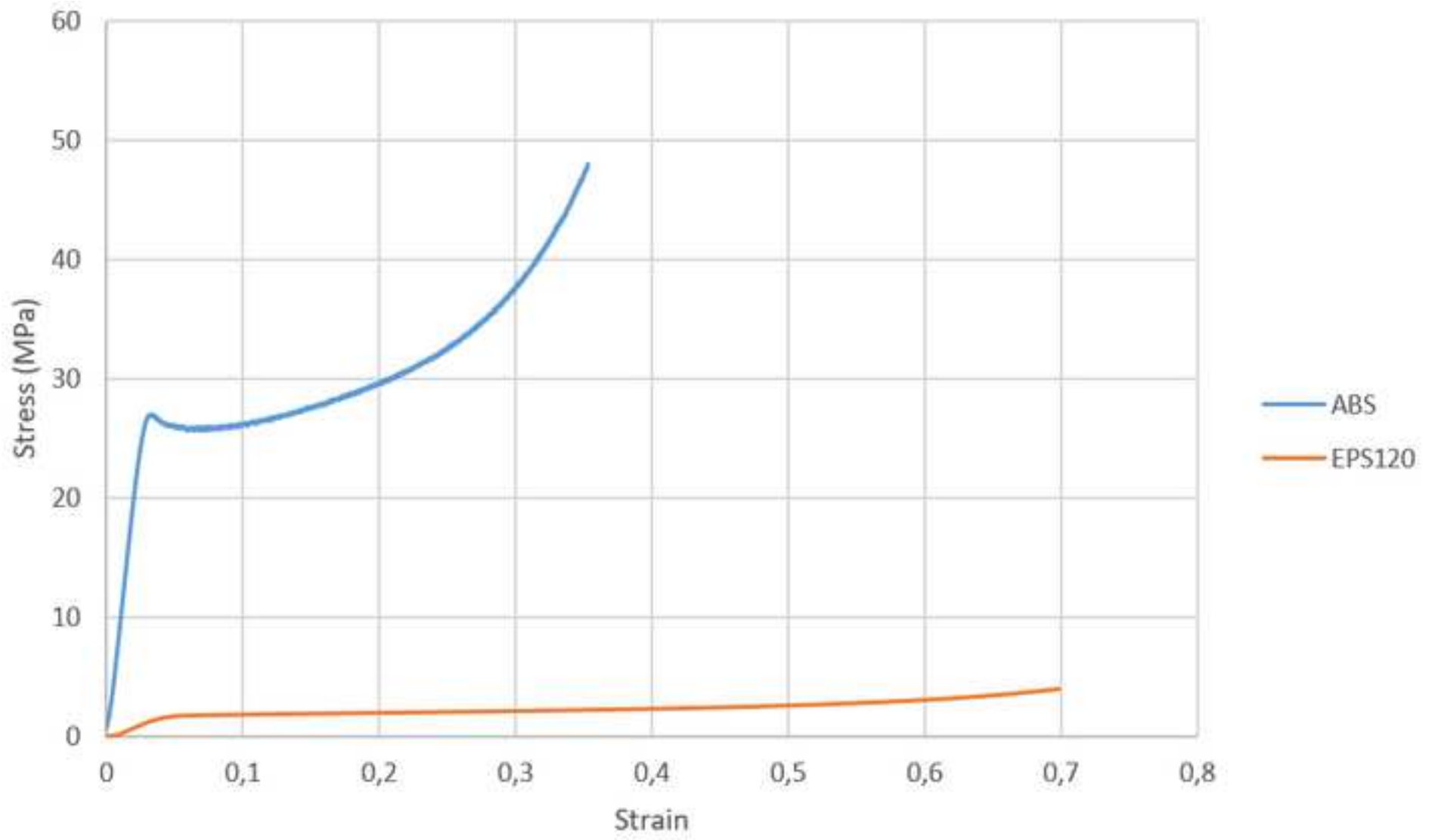


Fig. 4. Left: Typical stress–strain (left) and energy–stress (right) diagram of different materials

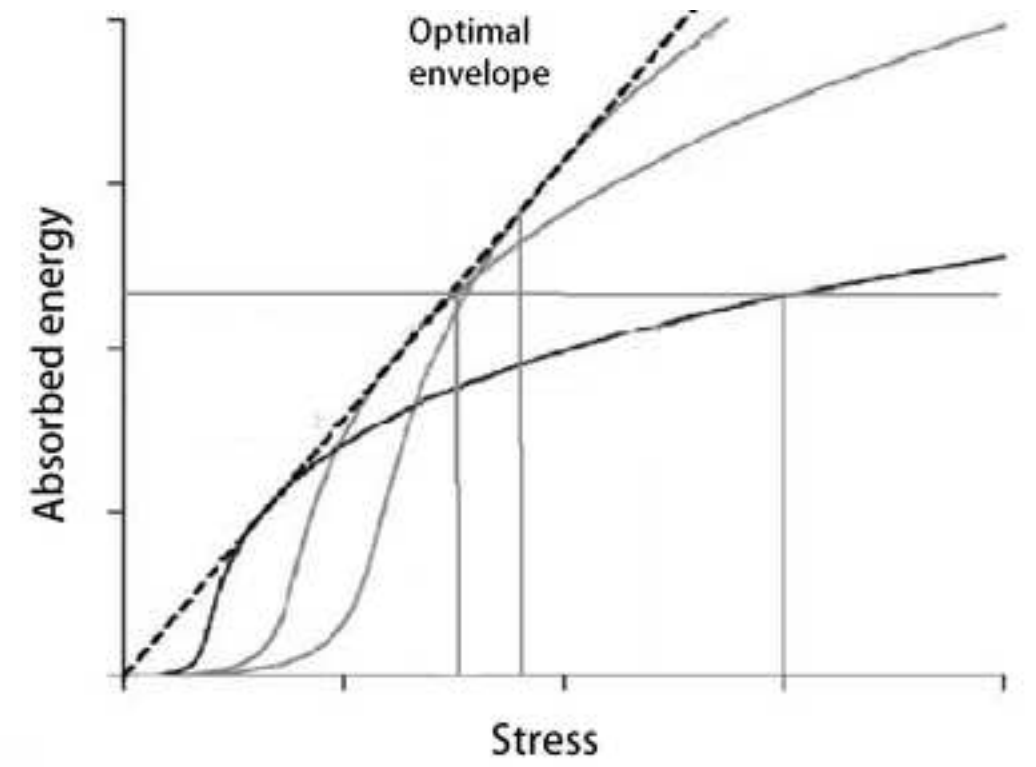
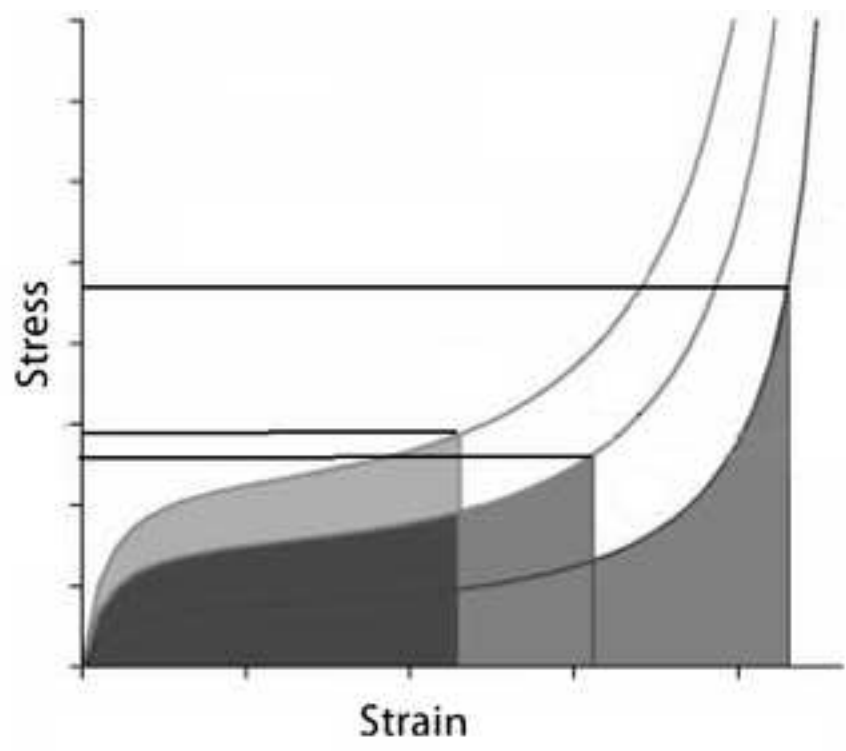


Fig. 5. Left: Typical efficiency–stress diagram of different materials. Right: Ideality–stress diagram and energy absorbed–stress diagram

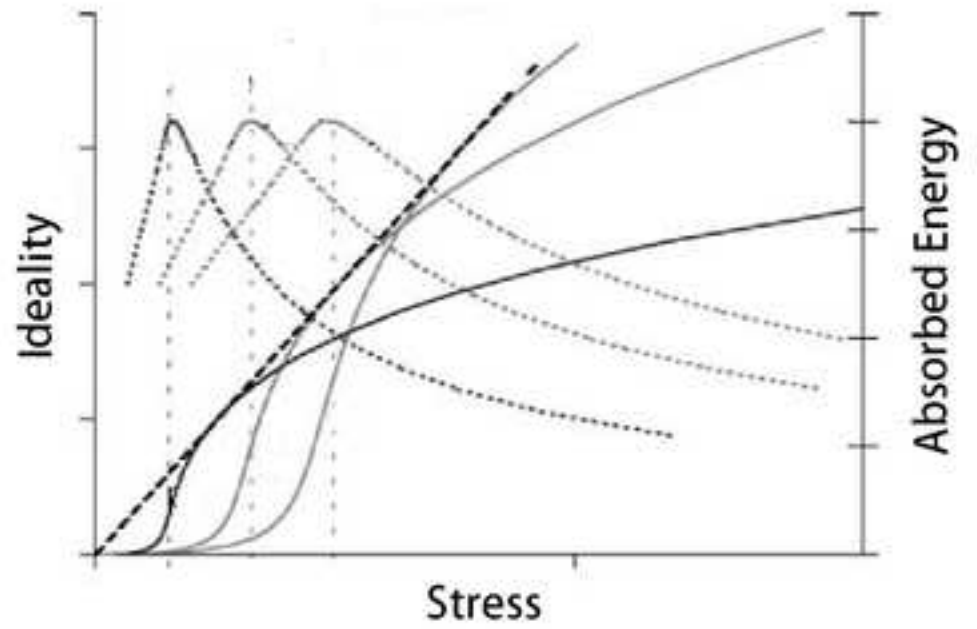
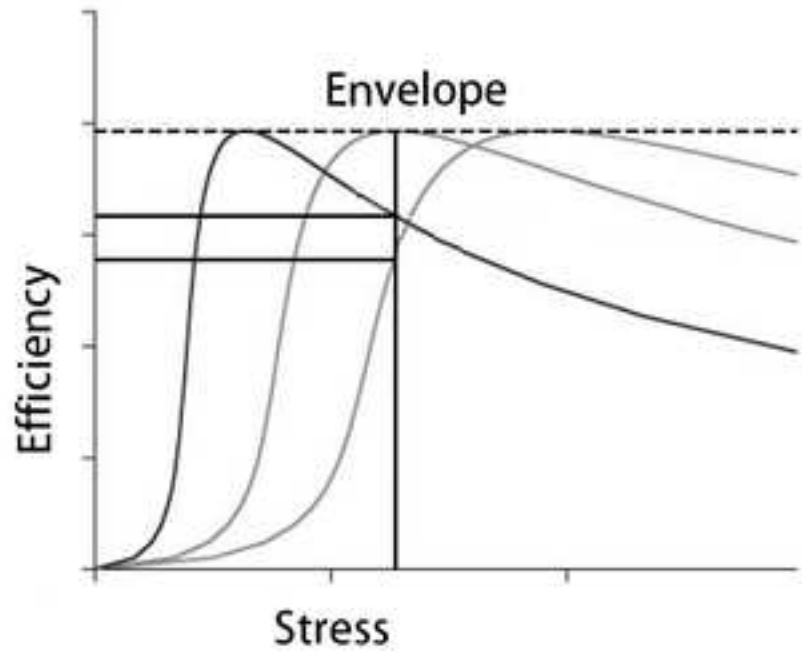


Fig. 6. Stress-strain compression curve for all the studied specimens

[Click here to access/download;Figure;fig_6.bmp](#)

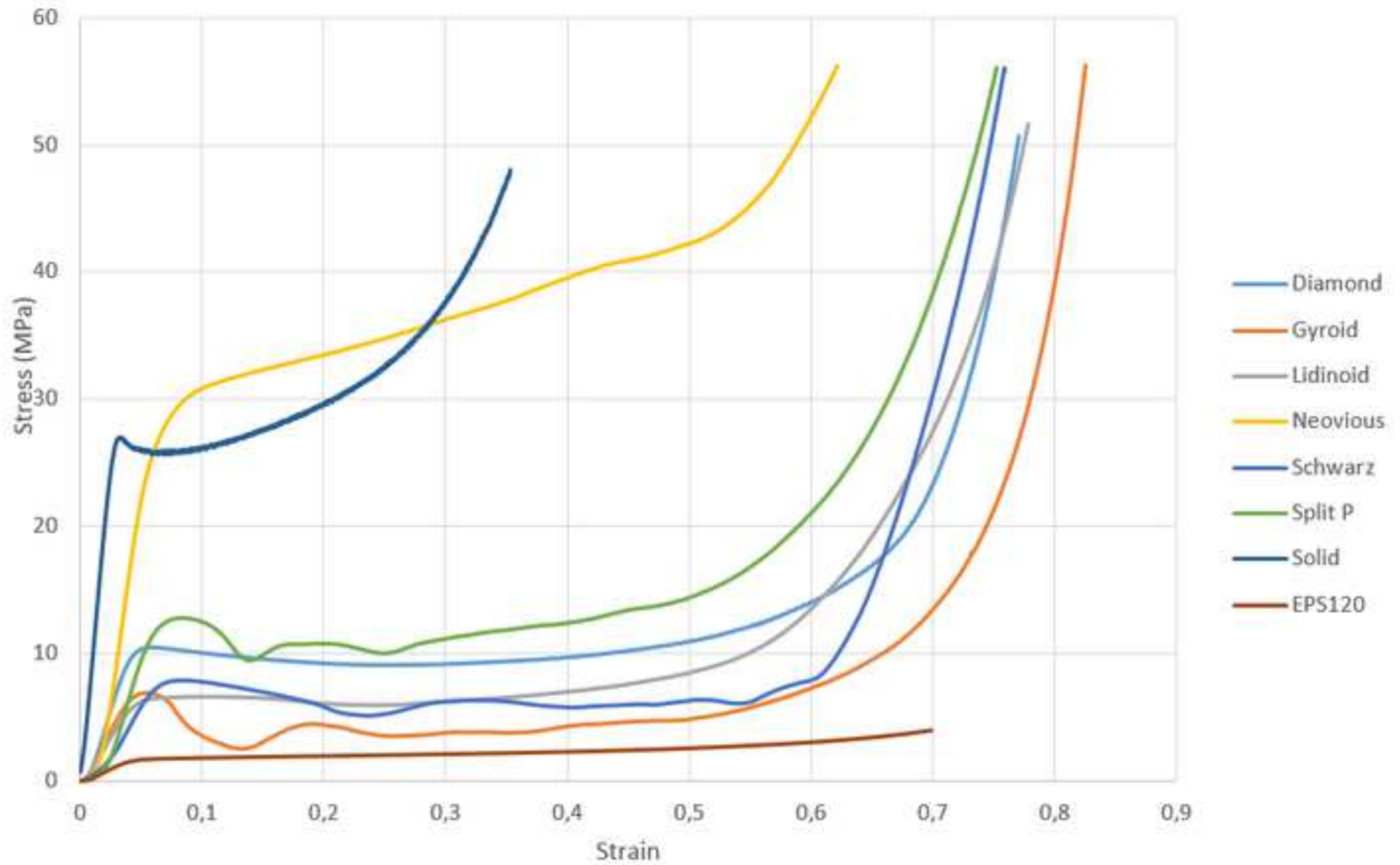


Fig. 7. Specific stress–strain compression curve for all the studied specimens

[Click here to access/download;Figure;fig_7.bmp](#)

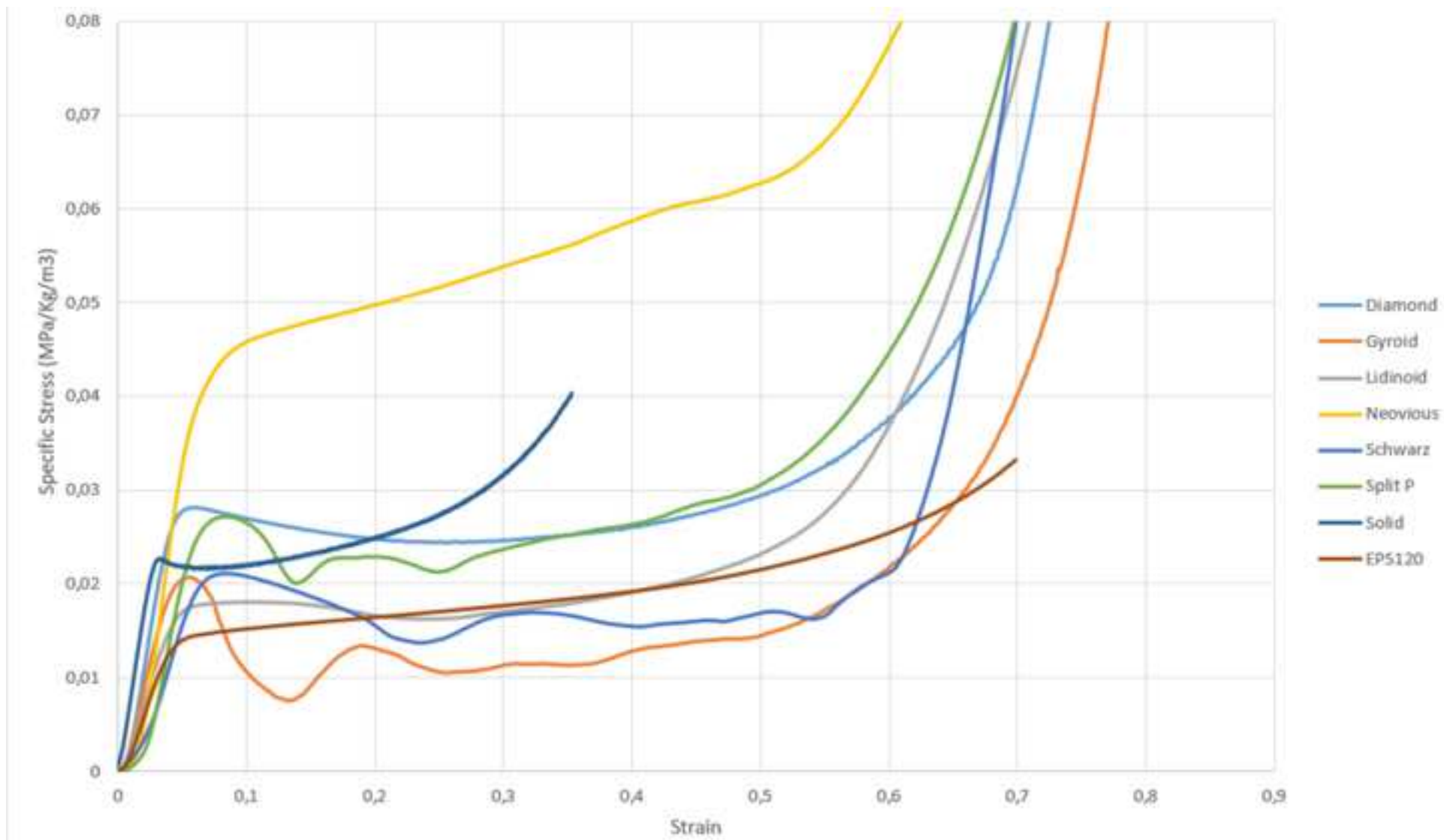


Fig. 8. Energy absorbed–strain compression curve for all the studied specimens

[Click here to access/download;Figure;Fig_8.bmp](#)

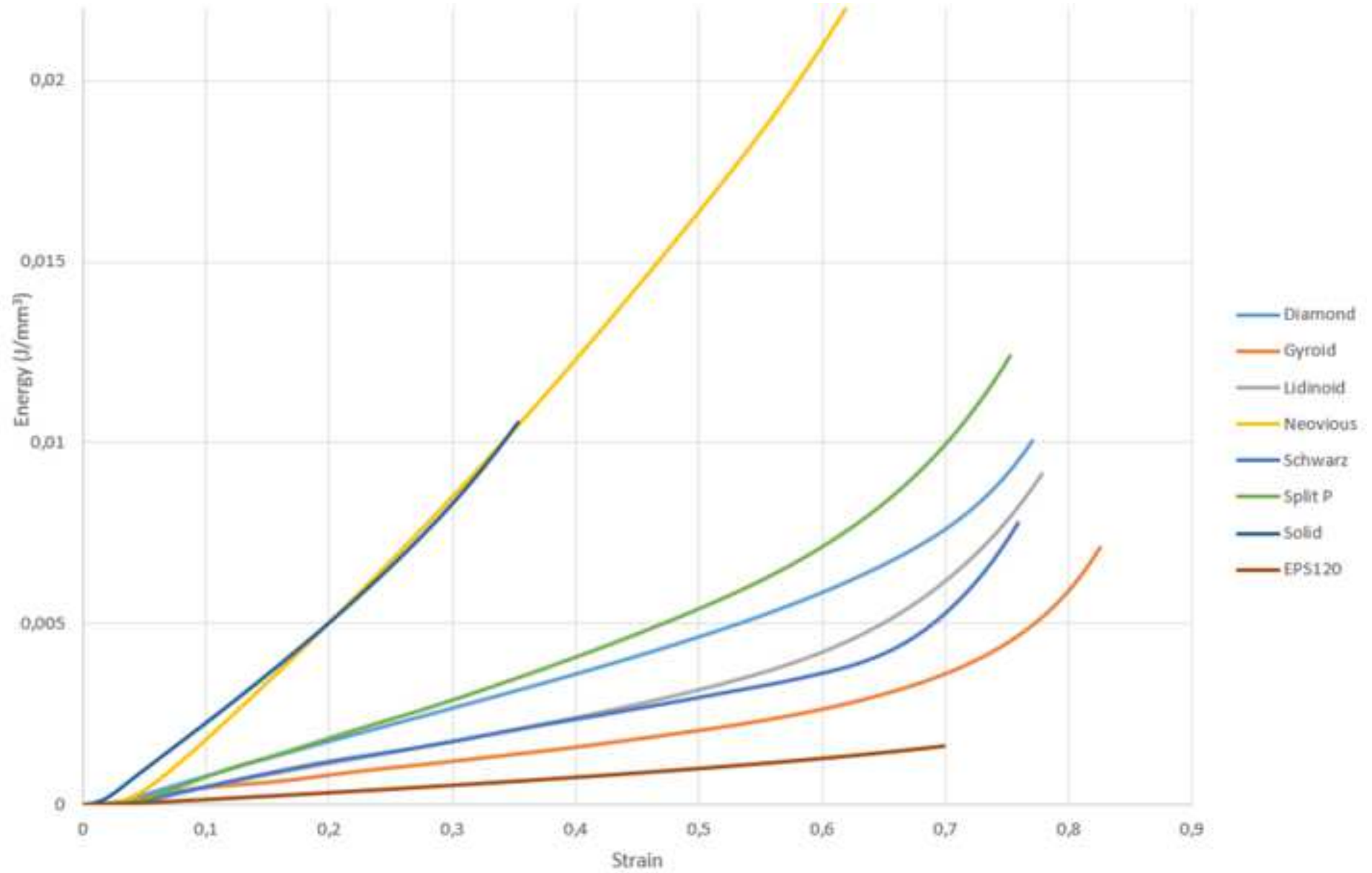


Fig. 9. Normalized energy–normalized stress for all the studied specimens

[Click here to access/download;Figure;fig_9.bmp](#)

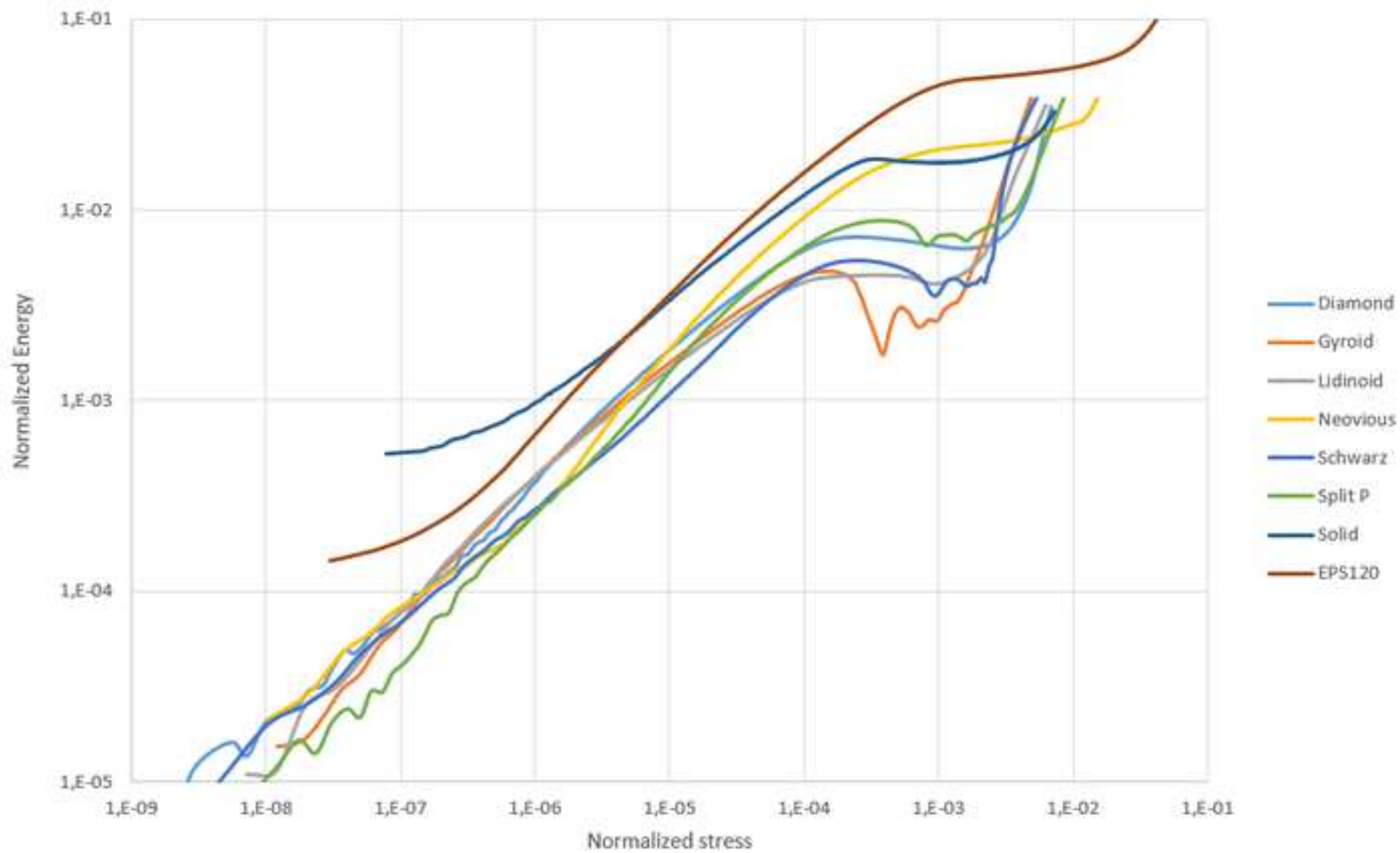


Fig. 10. Specific energy absorbed–strain compression curve for all the studied specimens

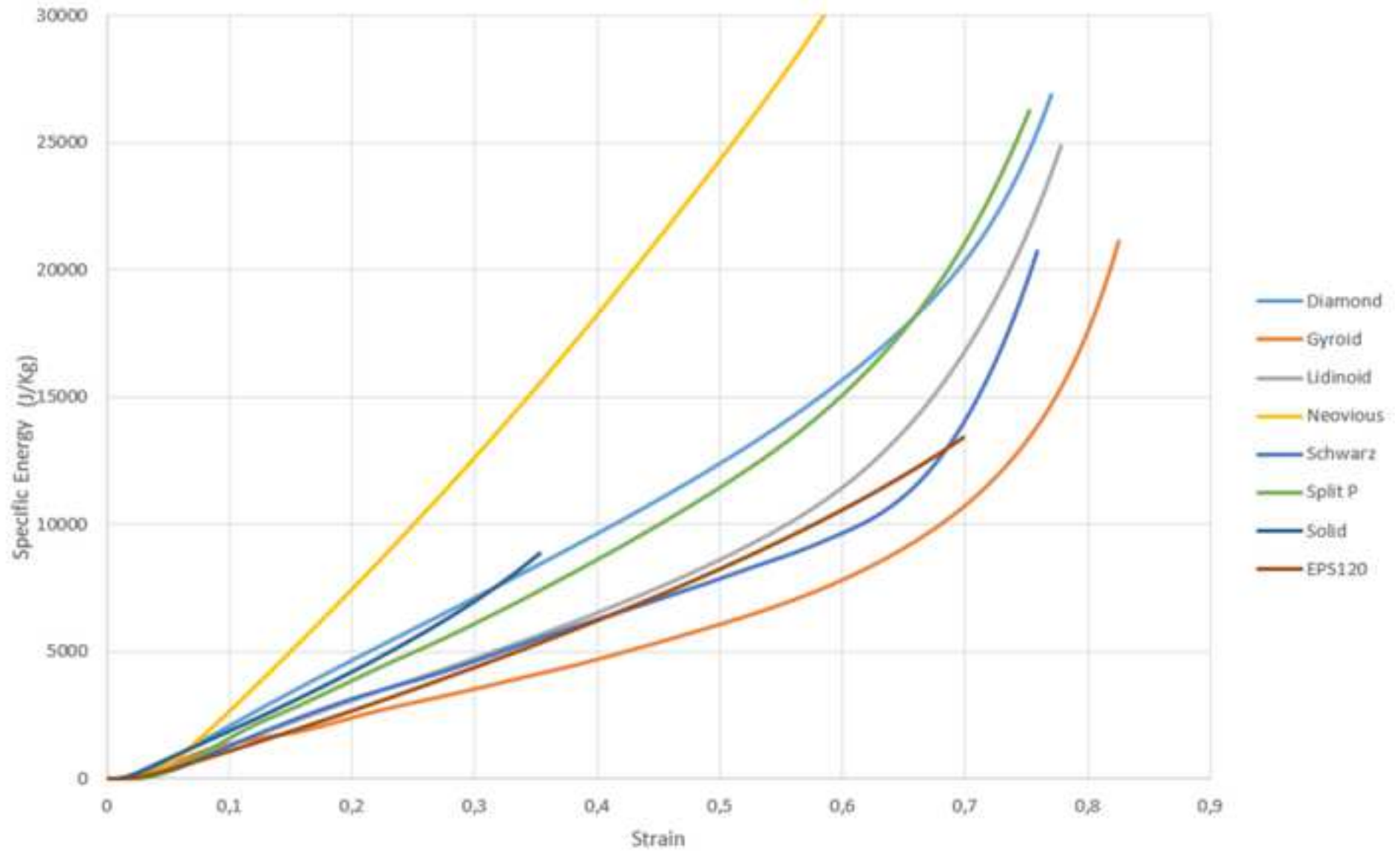


Fig. 11. Effectivity–stress (on logarithmic scale) for all the studied specimens

[Click here to access/download;Figure;fig_11.bmp](#)

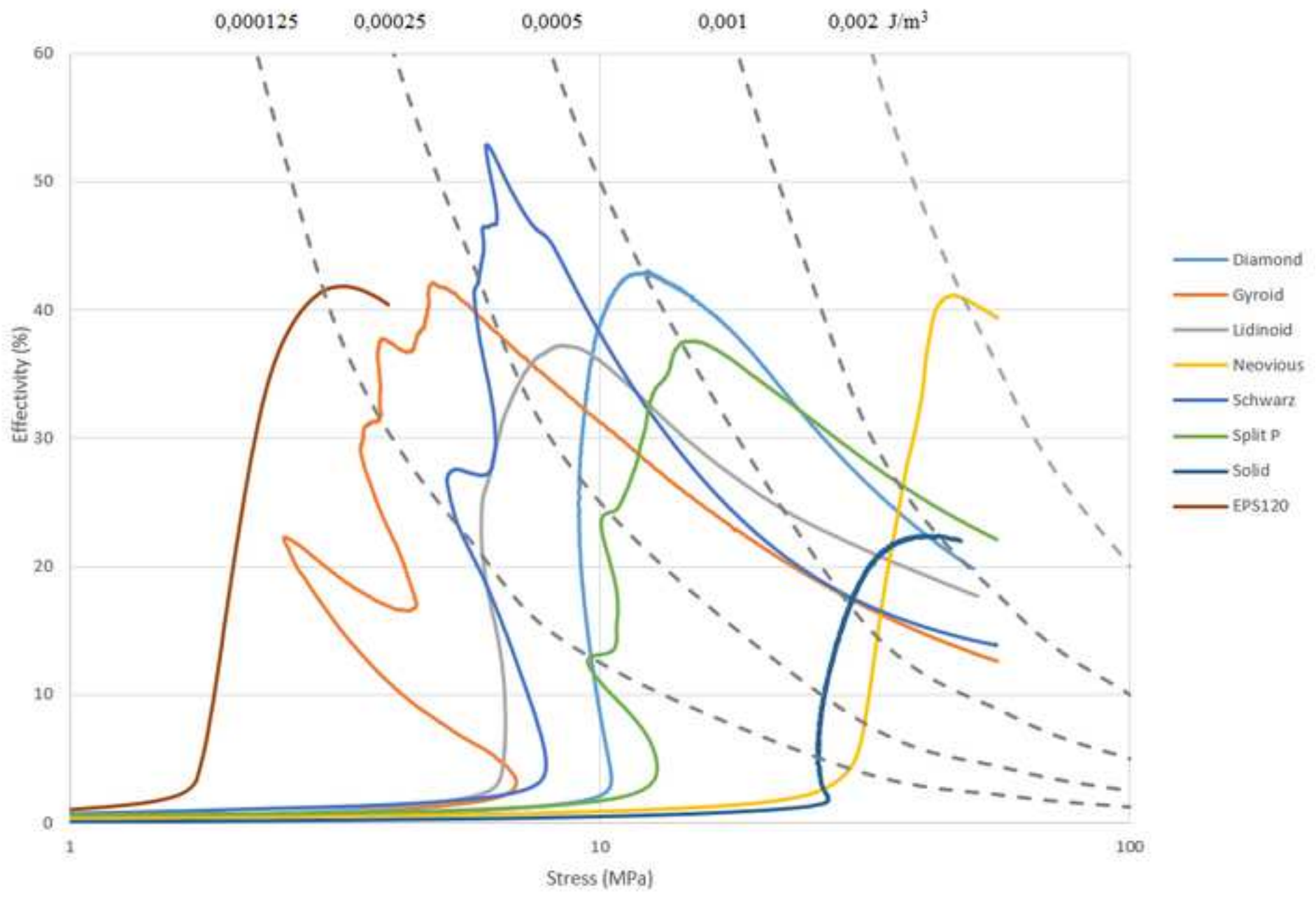


Fig. 12. Effectivity-strain for all the studied specimens

[Click here to access/download;Figure;fig_12.bmp](#)

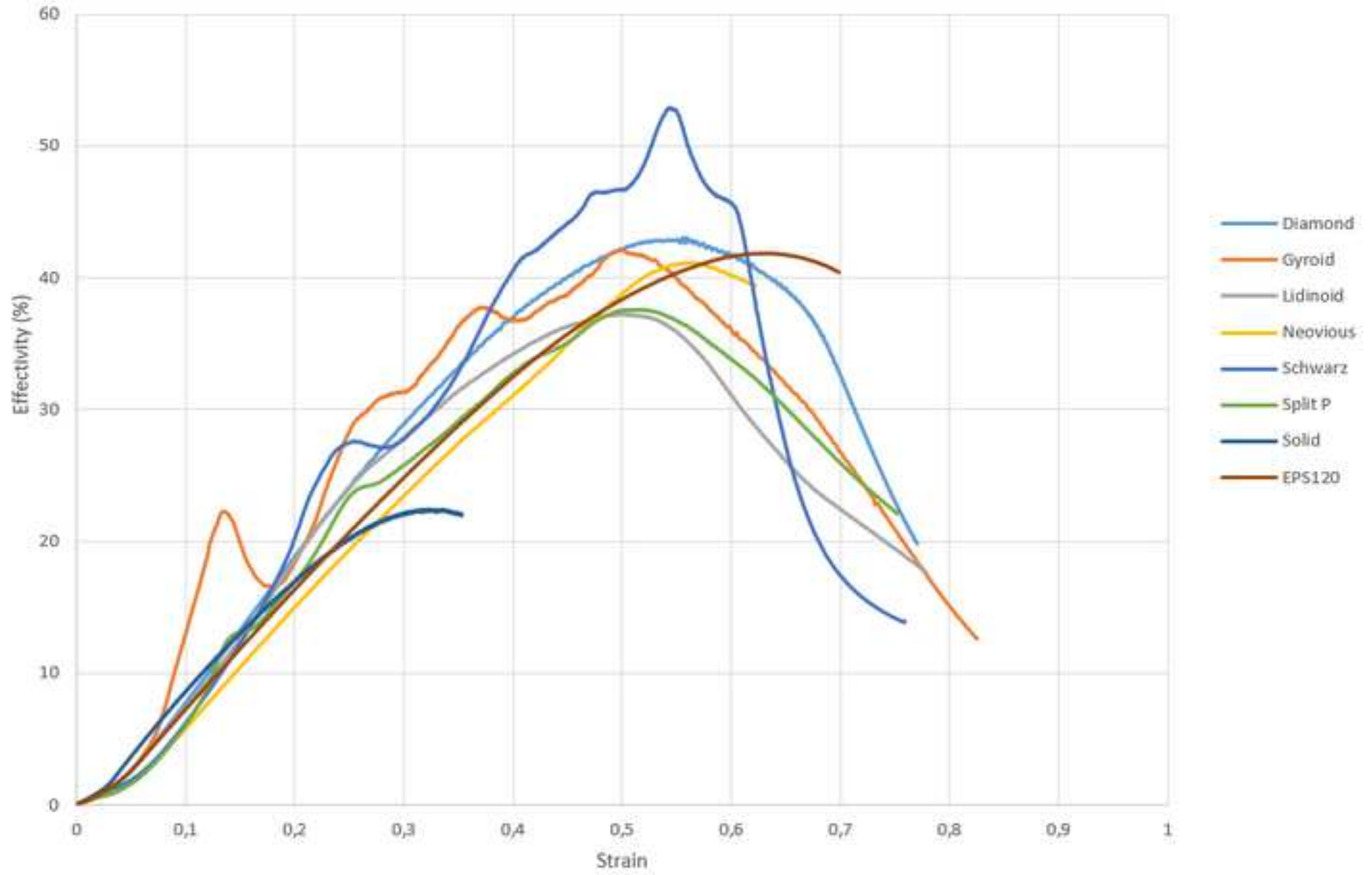


Fig. 13. Total effectivity–stress (on logarithmic scale) for all the studied specimens

[Click here to access/download;Figure;fig_13.bmp](#)

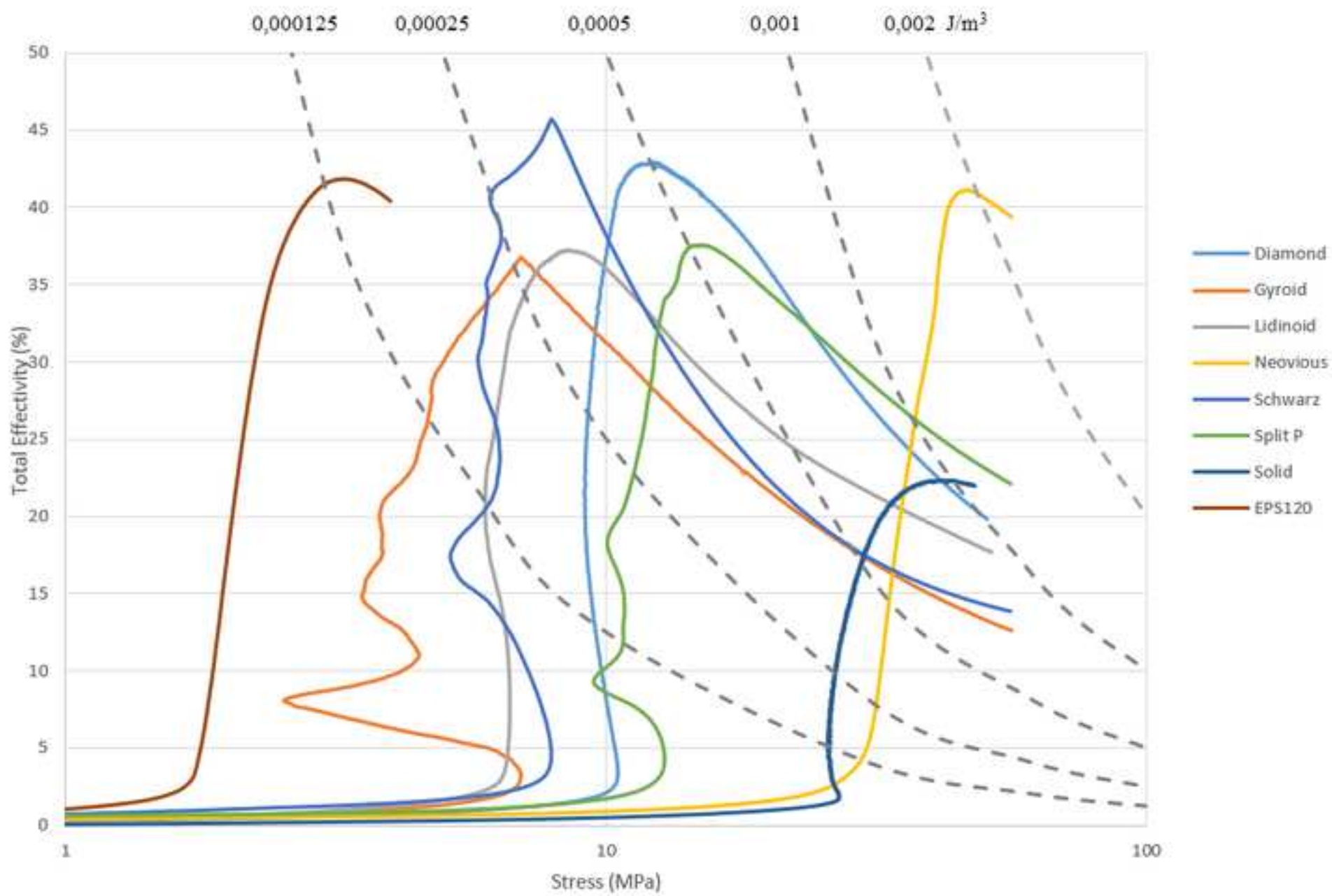


Fig. 14. Total effectivity–strain for all the studied specimens

[Click here to access/download;Figure;fig_14.bmp](#)

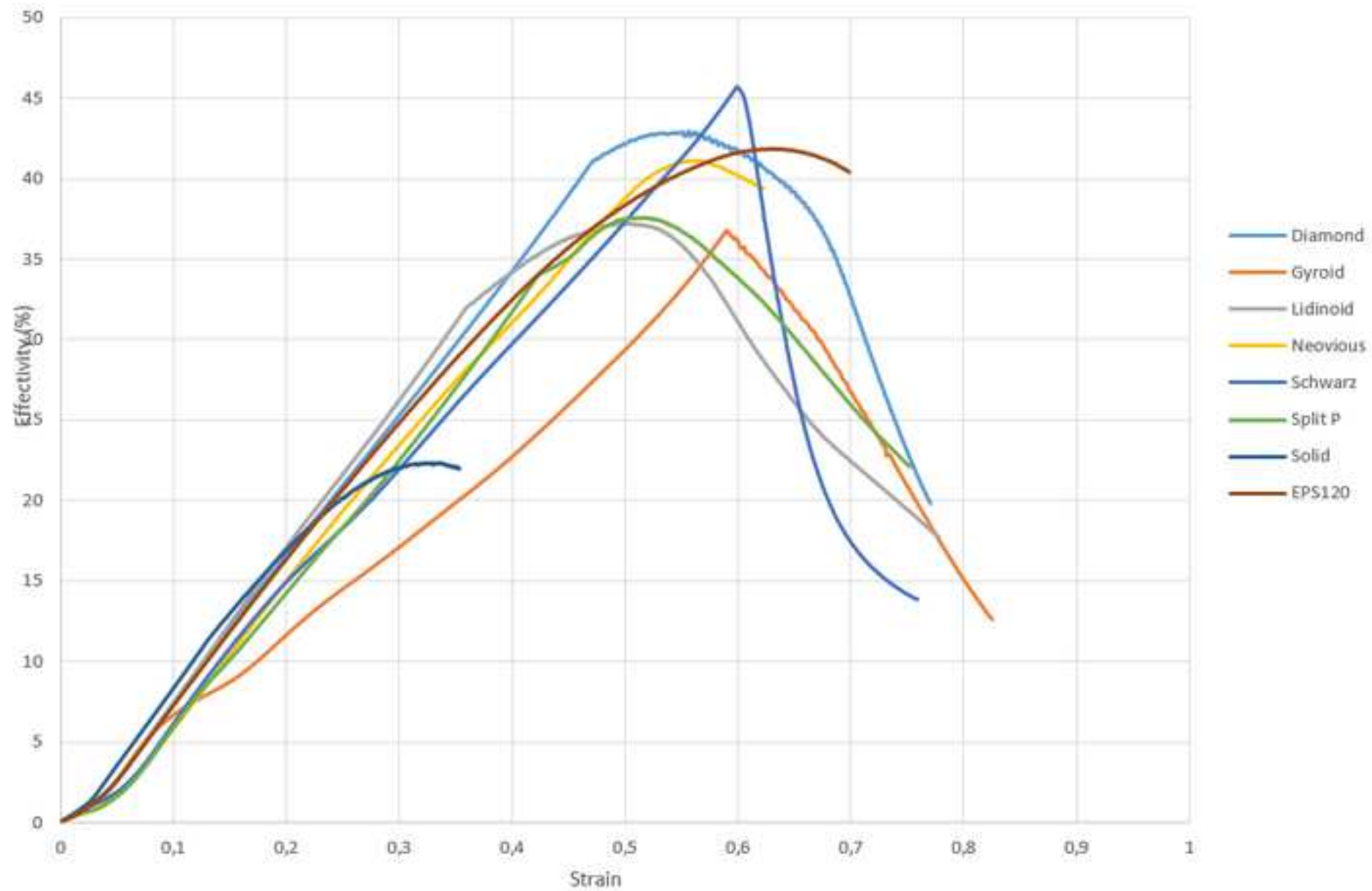


Fig. 15. Ideality–stress for all the studied specimens

[Click here to access/download;Figure;fig_15.bmp](#)

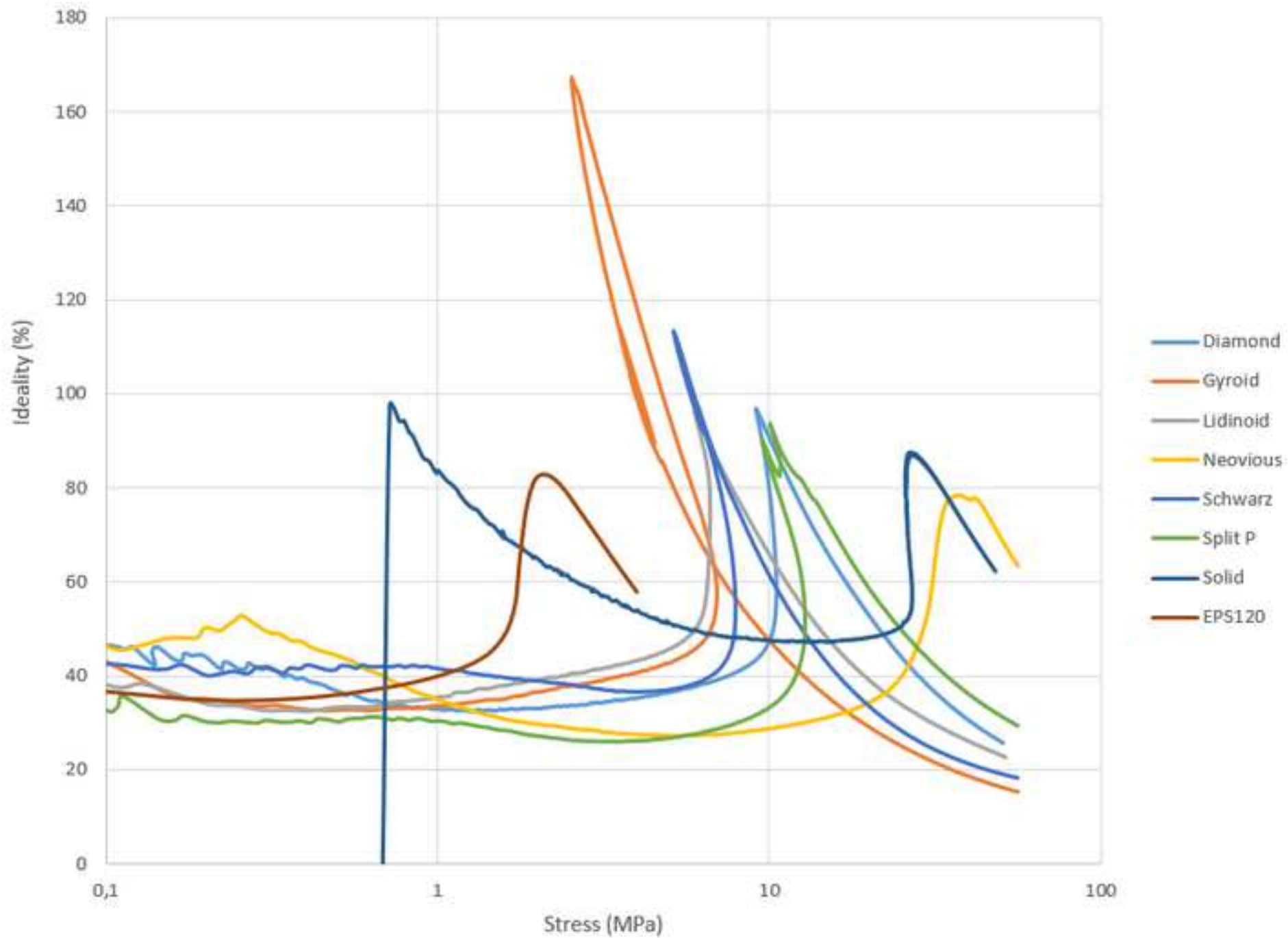
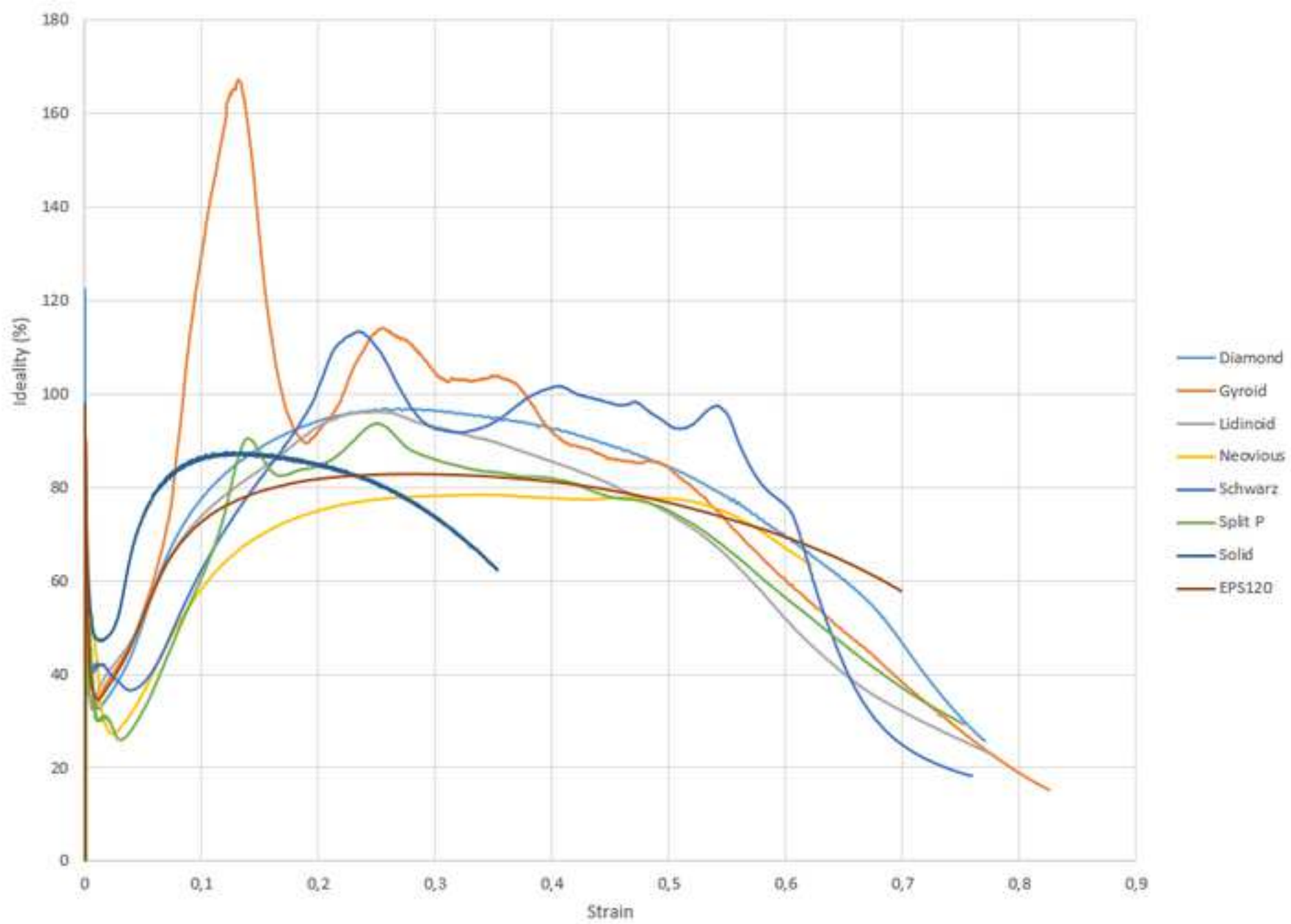


Fig. 16. Ideality–strain for all the studied specimens

[Click here to access/download;Figure;fig_16.bmp](#)



1
2
3
4
5
6
7
8
9
10
11
12
13
14
15
16
17
18
19
20
21
22
23
24
25
26
27
28
29
30
31
32
33
34
35
36
37
38
39
40
41
42
43
44
45
46
47
48
49
50
51
52
53
54
55
56
57
58
59
60
61
62
63
64
65



Click here to access/download
Table
table_1.docx

1
2
3
4
5
6
7
8
9
10
11
12
13
14
15
16
17
18
19
20
21
22
23
24
25
26
27
28
29
30
31
32
33
34
35
36
37
38
39
40
41
42
43
44
45
46
47
48
49
50
51
52
53
54
55
56
57
58
59
60
61
62
63
64
65




Click here to access/download
Table
table_2.docx

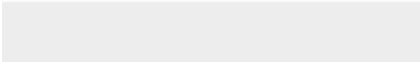



Table 3. Effectivity, total effectivity, ideality, and some related variables.

1
2
3
4
5
6
7
8
9
10
11
12
13
14
15
16
17
18
19
20
21
22
23
24
25
26
27
28
29
30
31
32
33
34
35
36
37
38
39
40
41
42
43
44
45
46
47
48
49
50
51
52
53
54
55
56
57
58
59
60
61
62
63
64
65



Click here to access/download
Table
table_3.docx



Declaration of interests

The authors declare that they have no known competing financial interests or personal relationships that could have appeared to influence the work reported in this paper.

The authors declare the following financial interests/personal relationships which may be considered as potential competing interests: